Volume 6 | Number 22 | 21 November 2014 | Pages 13257–14004

Nanoscale

www.rsc.org/nanoscale

ISSN 2040-3364

ROYAL SOCIETY OF CHEMISTRY

PAPER

Gianvito Vilé and Javier Pérez-Ramírez

Beyond the use of modifiers in selective alkyne hydrogenation: silver and gold nanocatalysts in flow mode for sustainable alkene production

NCNST

Nanoscale

PAPER

View Article Online
View Journal | View Issue

Cite this: *Nanoscale*, 2014, **6**, 13476

Beyond the use of modifiers in selective alkyne hydrogenation: silver and gold nanocatalysts in flow mode for sustainable alkene production†

Gianvito Vilé and Javier Pérez-Ramírez*

Received 20th May 2014,
Accepted 22nd July 2014

DOI: 10.1039/c4nr02777a

www.rsc.org/nanoscale

We report on the excellent stereo and chemoselectivity of nanosized silver and gold catalysts in the three-phase hydrogenation of acetylenic compounds under flow chemistry conditions. The materials featuring metal nanoparticles in the range of 2–21 nm were prepared by spray deposition or incipient wetness impregnation of silver nitrate and sol immobilisation of gold chloride on different carriers (Al_2O_3, SiO_2, TiO_2, and carbon), followed by activation in various atmospheres. The samples were characterised by ICP-OES, N_2 sorption, XPS, HAADF-STEM, and HRTEM, and evaluated in a continuous-flow flooded-bed micro-reactor. Both metals display optimal activities for particles below 5 nm, enabling stable operation at T = 373 K and P = 10 bar. While the performance of the silver catalysts is less influenced by the support, the gold nanoparticles exhibit significant activity only when deposited on TiO_2, likely due to the strong metal–support interaction. Hydrogenations of functionalised alkynes reveal that silver and gold match, and in some cases exceed, the selectivity of benchmark palladium-based catalysts. Furthermore, in contrast to Pd, the Ag and Au samples require no modifiers, which brings fundamental and practical simplifications for their understanding and large scale manufacture. Therefore, these materials could be advantageously used for the continuous production of olefinic intermediates in the fine chemical and pharmaceutical industries.

Introduction

Driven by the quest to reduce the use of hazardous compounds and stoichiometric reagents and maximise productivity, the search for innovation in the fine chemical and pharmaceutical industries has accelerated over the last decade.[1] An elegant approach for adapting current operations to more sustainable practices involves the application of continuous-flow reactors and ultra-selective heterogeneous catalysts.[2] For example, the liquid-phase semi-hydrogenation of acetylenic compounds is an important step for the industrial synthesis of *cis*-alkenes, essential building blocks for drugs, vitamins, fragrances, and agrochemicals,[3] and can benefit from the use of flow chemistry devices and novel catalytic systems. This reaction is usually carried out in (semi-)batch mode over Lindlar-type catalysts, which consist of 5 wt% palladium supported on calcium carbonate or barium sulfate, poisoned by lead, and sometimes further modified by quinoline.[4] On the other hand, continuous-flow fixed-bed micro-reactors can offer a number of advantages, such as improved mass and heat transfer and controlled residence time, enabling the attainment of superior product selectivity and a high space time yield, a more efficient energy use due to a better temperature control, and the possibility of intensified processes by applying numbering-up and scaling-out principles.[5] Besides, the suboptimal utilisation of the high content of palladium[6] and the presence of toxic additives (*i.e.*, lead and quinoline) in the catalyst formulation encourage the search for more environmentally-friendly materials.[7] The emergence of ligand-modified palladium nanoparticles as a lead-free alternative to the Lindlar catalyst and with an order of magnitude lower palladium loading, has received increasing attention due to the excellent degree of alkene selectivity in the hydrogenation of short-chain alkynes and alkynols.[8] However, the organic ligand attached to the Pd nanoparticle surface imposes severe access and adsorption constraints in the reduction of bulkier acetylenic compounds with internal C≡C unsaturations,[9] limiting its scope of application. Therefore, the development of catalysts surpassing the performance of palladium-based systems constitutes a challenge which requires the identification of new active metals.

An alternative approach for catalysing the semi-hydrogenation of alkynes comprises the use of non-modified metal nanoparticles which do not readily activate hydrogen. The limited H coverage and hydride formation can hinder unde-

Institute for Chemical and Bioengineering, Department of Chemistry and Applied Biosciences, ETH Zurich, Vladimir-Prelog-Weg 1, 8093 Zurich, Switzerland. E-mail: jpr@chem.ethz.ch

†Electronic supplementary information (ESI) available. See DOI: 10.1039/c4nr02777a

sired reaction pathways, such as over-hydrogenation and isomerisation. For example, silver and gold nanoparticles have shown an excellent selectivity in the gas-phase hydrogenation of ethyne, propyne and 1,3-butadiene, owing to the preferential adsorption of the triple bond at the edges of the metal nanoparticles.[10,11] However, high operating temperatures (*ca.* 600 K) are required and hence these catalysts cannot be retrofitted in existing olefin purification plants. The conversion of acetylenic substrates over these metals in the liquid phase and flow mode has not been reported thus far. Yamamoto and co-workers have studied the performance of bulk gold foils (5 × 2 mm) in the three-phase hydrogenation of acetylenic compounds, using organosilane as the hydrogen source and moderate temperatures and pressures.[10b] The authors claimed that gold cannot catalyse the reaction unless hydrogen atoms are supplied to the metal surface by dehydrogenation of organic moieties and proton discharge.[10b] However, metal nanoparticles with well-defined surface defects (*e.g.*, steps, edges and kinks) can exhibit catalytic properties unobservable over bulk metals, including an enhanced H_2 activation,[12] which can improve the hydrogenation ability of Ag and Au-based catalysts.

In this work, we have assessed the performance of supported silver and gold nanoparticles with tailored size for the three-phase hydrogenation of alkynes under flow chemistry conditions. The excellent alkene selectivity over Ag and Au has been compared with that of state-of-the-art Pd-based catalysts. The results provide insights into the design of efficient modifier-free hydrogenation catalysts that can be applied for continuous manufacture of *cis*-alkenes in the fine chemical and pharmaceutical industries.

Experimental details

Catalyst preparation

A series of silver and gold-based catalysts supported on SiO_2 (Evonik, 99.8%), TiO_2-anatase (Sigma-Aldrich, 99.7%), γ-Al_2O_3 (Merck, 99%), and activated carbon (Sigma-Aldrich, Norit), were prepared. Silver catalysts with a nominal metal loading of 1 wt% were synthesised by spray deposition and incipient wetness impregnation using $AgNO_3$ (Sigma-Aldrich, 99.9%) as the silver precursor. The spray deposition method[13] was performed with a Büchi Mini Spray Dryer B-290 equipped with a two-fluid nozzle of 1.4 mm in diameter. This technique enables the deposition of supported nanoparticles with high metal dispersion and uniform particle size distribution. In fact, the confined growth and instant drying during the synthesis enable to control the particle size, avoiding undesired agglomeration and redispersion of the metal species during the crystallisation on the support.[11b,13] Silver nitrate (0.03 g) was dissolved in deionised water (20 cm^3), followed by the addition of the support (2 g). The resulting suspension was pumped at 3 cm^3 min^{-1} into the two-fluid nozzle, together with a spray air flow of 0.5 m^3 h^{-1}. The inlet temperature was set at 493 K, the aspiration rate at 35 m^3 h^{-1}, and the outlet temperature was 383 K. The dried particles were separated in a cyclone. The incipient wetness impregnation was performed by dissolving silver nitrate (0.016 g) in deionised water (1.5 cm^3) and by adding SiO_2 (1 g) to the solution. The resulting powder was dried in a Labconco FreeZone Plus 2.5 L Cascade Benchtop Freeze Dry System at 40 K and 0.02 bar. In order to vary the average silver particle size, the silver catalysts after spray deposition and incipient wetness impregnation were activated in static air or flowing N_2 or 5 vol% H_2/He (42 cm^3 min^{-1}), at different conditions of temperature and time (Table 1), using a heating rate of 5 K min^{-1}. The gold catalysts were prepared by sol immobilisation.[14] $HAuCl_4 \cdot 3H_2O$ (0.05 g, ABCR-Chemicals, 99.99%) was dissolved in deionised water (1 cm^3), followed by the addition of an aqueous solution of 2 wt% PVA (ABCR-Chemicals, 98–99%) (PVA/Au mass ratio = 1). The resulting emulsion was mixed with a solution of 0.1 M $NaBH_4$ (Sigma-Aldrich, >96%) ($NaBH_4$/Au mass ratio = 1), forming Au^0 colloidal nanoparticles. The colloids were immobilised by addition of the support under vigorous magnetic stirring for 2 h. The amount of support was calculated to reach a nominal Au loading of 1 wt%. The slurry was filtered and the solids were washed with deionised water, dried at 383 K for 24 h, and activated under flowing N_2 (42 cm^3 min^{-1}) at 623–1173 K for 3 h (heating rate = 5 K min^{-1}). The reference gold catalyst (1 wt% Au/TiO_2, S_{BET} = 51 m^2 g^{-1}, Strem Chemicals, ref: 79-0165), the Lindlar catalyst (5 wt% Pd 3 wt% Pb/$CaCO_3$, S_{BET} = 10 m^2 g^{-1}, Alfa Aesar, ref: 043172), and the NanoSelect™ catalyst (0.6 wt% Pd–HHDMA/C, S_{BET} = 336 m^2 g^{-1}, Strem Chemicals, ref: 46-1710) were used as received. 20 wt% CeO_2/TiO_2 was prepared by wet impregnation in HNO_3 solution.[15]

Catalyst characterisation

The silver and gold content in the solids was determined by inductively coupled plasma optical emission spectrometry (ICP-OES) using a Horiba Ultra 2 instrument. Nitrogen isotherms at 77 K were measured in a Micromeritics TriStar II instrument. High-angle annular dark-field scanning transmission electron microscopy (HAADF-STEM) and high-resolution transmission electron microscopy (HRTEM) were undertaken in a FEI Tecnai F30 FEG operated at 300 kV. The size distribution of gold or silver nanoparticles was assessed by analysing *ca.* 300 individual nanoparticles and the corresponding degree of dispersion was estimated by considering particles to be truncated octahedrons with cubic symmetry. X-ray photoelectron spectroscopy (XPS) was performed on a VG-Microtech Multilab 3000 spectrometer featuring a hemispheric electron analyser with 9 channeltrons and non-monochromatised Al Kα radiation at 1486.6 eV. The catalysts were pretreated at 393 K under flowing He (20 cm^3 min^{-1}) for 60 min, and reduced *in situ* at 348 K under flowing 5 vol % H_2/He (20 cm^3 min^{-1}) for 30 min. The spectra were collected under ultra-high vacuum conditions (residual pressure of *ca.* 5 × 10^{-8} Pa) at a pass energy of 50 eV. All binding energies were referenced to the C 1s level at 284.6 eV in order to compensate for charging effects.

Catalyst testing

The three-phase hydrogenation of acetylenic compounds was carried out in a fully-automated continuous-flow flooded-bed

Table 1 Characterisation data of the silver and gold-based catalysts

Code	Catalyst	Preparation[a]	Ag or Au[b] (wt%)	S_{BET} (m^2 g^{-1})	$d_{particle}$[c] (nm)	D^c (%)
A	Ag/SiO_2	SD, H_2 flow, 473 K, 0.5 h	1.3	196 (197)[d]	4.4 ± 3.1	24
B		IW, N_2 flow, 473 K, 0.5 h	1.3	196	2.0 ± 0.3	54
C		SD, static air, 573 K, 2 h	1.3	196	21.3 ± 8.3	5
D	Ag/TiO_2	SD, H_2 flow, 473 K, 0.5 h	1.0	58	2.8 ± 0.2	49
E	Ag/Al_2O_3	SD, H_2 flow, 473 K, 0.5 h	0.9	79 (78)	2.3 ± 0.8	45
F	Au/SiO_2	SI, N_2 flow, 623 K, 3 h	0.9	164	6.0 ± 1.4	19
G	Au/TiO_2	SI, N_2 flow, 623 K, 3 h	1.0	60 (57)	2.7 ± 0.7	46
H		SI, N_2 flow, 923 K, 3 h	1.0	54	3.7 ± 0.9	31
I		SI, N_2 flow, 1023 K, 3 h	1.0	52	8.1 ± 3.3	14
J		SI, N_2 flow, 1173 K, 3 h	1.0	52	21.0 ± 5.3	5
K	Au/C	SI, N_2 flow, 623 K, 3 h	1.0	1365 (1341)	3.5 ± 1.2	33

[a] Synthesis technique and atmosphere, temperature, and time of activation. SD: spray deposition; IW: incipient wetness impregnation; SI: sol immobilisation. [b] Metal content, determined by ICP-OES. [c] Average metal particle size, $d_{particle}$, and metal dispersion, D, determined by HAADF-STEM. [d] Total surface area of the carriers between brackets.

micro-reactor (ThalesNano H-Cube Pro™), in which the liquid alkyne and the gaseous hydrogen flow concurrently upward through a fixed bed of catalyst particles.[9] The catalyst (0.5 g for the Ag and Au catalysts, 0.1 g for the Pd catalysts, and 0.85 g for the CeO_2 catalyst, particle size: 0.2–0.4 mm) was loaded into a cartridge of approximately 0.35 cm internal diameter. The acetylenic substrates included 1-hexyne (Acros Organics, 98%), 3-hexyne (TCI Deutschland, 98%), 2-methyl-1-buten-3-yne (ABCR-Chemicals, 97%), 2-methyl-3-butyn-2-ol (Acros Organics, 98%), phenylacetylene (Acros Organics, 98%), 9-dodecyn-1-ol (ABCR-Chemicals, 98%), 1,1-diphenyl-2-propyn-1-ol (Sigma-Aldrich, 99%), and 3-butyn-2-one (ABCR-Chemicals, 97%). Unless specified, reaction solutions contained 1 vol% of alkyne in toluene (Acros Organics, 99.9%) as solvent. When assessing the influence of the feed concentration of 1-hexyne on the catalytic performance, the amount of substrate was varied in the range of 1–100 vol%; in case of alkyne–alkene mixtures, the solutions contained 1 vol% of 1-hexyne and 1 vol % of 1-hexene (Fluka-Chemie, >97%) in toluene. The hydrogenation reactions were performed at various conditions of temperature (293–373 K), total pressure (1–40 bar), and liquid (alkyne + solvent and, if applicable, also the alkene: 0.3–3 cm^3 min^{-1}) and H_2 (3–60 cm^3 min^{-1}) flow rates. At these conditions, the possible metal leaching during reaction can be ruled out. The reaction products were collected after reaching steady-state operation (in *ca.* 20 min), and analysed offline using a HP 6890 gas chromatograph equipped with a HP-5 capillary column and a flame ionisation detector. The conversion (X) of alkyne was determined as the amount of reacted alkyne divided by the amount of alkyne at the reactor inlet and the selectivity (S) to the alkene/alkane was quantified as the amount of the particular compound divided by the amount of reacted alkyne. The reaction rate (r) was expressed as mole of alkene produced per mass of catalyst and unit of time.

Results and discussion

The total surface area of the support is retained upon incorporation of the metal phase (Table 1). In addition, the actual loading of silver and gold, determined by ICP-OES, is close to the nominal value (1 wt%). The smallest Ag and Au nanoparticles are observed for 1 wt% Ag/SiO_2 prepared by spray deposition and activated in N_2 flow at 473 K for 0.5 h (catalyst **B**, $d_{particle}$ = 2.0 nm), and for 1 wt% Au/TiO_2 prepared by sol immobilisation and activated in N_2 flow at 623 K for 5 h (catalyst **G**, $d_{particle}$ = 2.7 nm). The activation step of the supported catalysts has a marked influence on the metal particle size. In fact, the use of a static air atmosphere for the silver catalysts (code **C**) and the increase of the activation temperature for the gold catalysts (codes **H**, **I**, **J**) lead to larger particles (from 4 to 21 nm, corresponding to dispersion values ranging from 31 to 5%, respectively). Therefore, by controlling the activation conditions, it is possible to tune the size of the silver and gold nanoparticles. The carrier was also varied during the preparation, but only slight changes in particle size are detected over the catalysts activated under similar conditions (codes **A**, **D**, **E** for silver and **F**, **G**, **K** for gold). This suggests that the support has a relatively minor influence on stabilising small

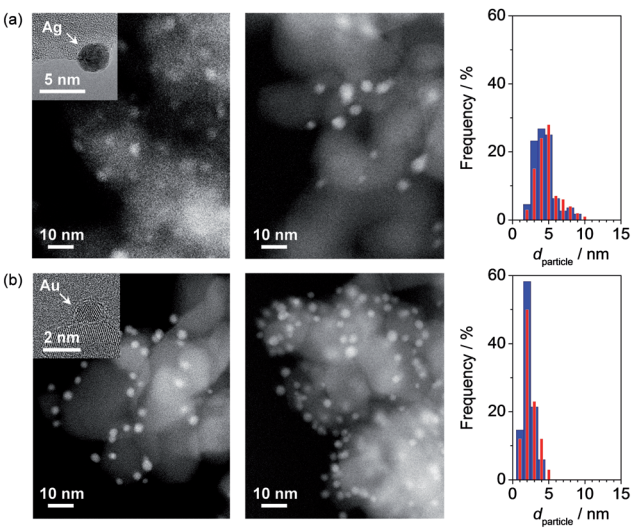

Fig. 1 HAADF-STEM micrographs of the fresh (left) and used (middle) catalysts and respective particle size distributions (right) of **A** (a) and **G** (b) in Table 1. The insets in the left images show HRTEM of the samples.

nanoparticles. Fig. 1 shows representative high-resolution HAADF-STEM micrographs and the associated particle size distributions of selected Ag and Au-based catalysts with catalytically-optimal average diameter (*vide infra*). The images show that the nanoparticles have spherical shapes, resembling the structure of the standard Wulff truncated cubo-octahedra,[16] with mono-disperse size distribution. This nanoparticle morphology is largely preserved upon hydrogenation, as confirmed by the microscopy analyses of the used catalysts (Fig. 1). The XPS measurements (Fig. 2) evidence two different Ag $3d_{5/2}$ binding energies at 368 and 371 eV for Ag/SiO_2, and a distinct Au $4f_{7/2}$ binding energy at 83.8 eV for Au/TiO_2, indicating that the surface of Ag is partially oxidised while that of Au is fully metallic.[17] This result is confirmed for the other supported catalysts (Fig. S1†). In particular, the amount of oxidic silver depends on the type of support and increases with the order: $Ag/SiO_2 < Ag/TiO_2 < Ag/Al_2O_3$.

The various nanocatalysts were first evaluated in the continuous-flow three-phase hydrogenation of 1-hexyne. Fig. 3a depicts the catalytic performance as a function of the average metal size. The reaction rate over the Ag and Au-based catalysts increases when the particle size is increased from 2 to 5 nm, and abruptly decreases for larger particles. In the case of Ag, the figure shows the expected volcano dependence with a maximum at 4.5 nm, indicating that B5 sites are active centres of the reaction.[11b] For the gold samples, smaller nanoparticles of around 2–3 nm are required. On the other hand, the selectivity to 1-hexene is size independent, being higher than 95%. These findings are in line with earlier studies on the structure-sensitivity of silver and gold-catalysed gas-phase alkyne hydrogenation, which suggested that the reaction follows the Horiuti–Polanyi mechanism over gold and an alkyne-assisted H_2 splitting mechanism over silver.[10,11b] Varying the type of carrier (Fig. 3b), the SiO_2 and C-supported Au catalysts show remarkably lower activities than 1 wt% Au/TiO_2. Considering the equivalent particle size distribution of 1 wt% Au/C and catalyst **H** (Table 1) and the different performance (Fig. 3a and b), this drop cannot be attributed to the distinct average gold size in the catalysts. Therefore, it suggests that the strong metal–support interaction between the gold nanoparticles and the reducible TiO_2 carrier enhance the reactivity of Au, in agreement with the literature.[10c] In the case of silver, the reaction rate and the selectivity to 1-hexene are less dependent on the type of support, although SiO_2 appears as the best material, most likely because it contains a higher amount of metallic silver (Fig. S1†). Fig. 3c and d display the effects of temperature and total pressure on the performance of Au/TiO_2 and Ag/SiO_2 catalysts featuring 2.7 and 4.4 nm particles, respectively. The reaction rate increases with the increased temperature and pressure. However, this increase in activity at high operating conditions slightly affects the selectivity to 1-hexene (>95%). Finally, the effect of the liquid and H_2 flow rates on the catalytic activity are displayed in Fig. S2a and b.† As expected, the increase of the liquid flow rate decreases the catalytic activity because of the reduced contact time between the reactants and the catalyst. Similarly, the decrease of the H_2 flow rate has an adverse effect on the reaction rate. In all cases, the catalysts retain the high alkene selectivity in a broad range of experimental conditions. The contour plot in Fig. 4 better highlights the activity and selectivity window for the hydrogenation of 1-hexyne (A). Only at $P > 40$ bar, *n*-hexane is formed (B). Potentially, the absence of over-hydrogenated products and oligomers might be due to the low concentration of alkyne in the reaction solution. For this reason, we have conducted an additional experiment, varying the concentration 1-hexyne in the feed and reaching solvent-free conditions (Fig. S2c†). Also in these cases, the silver and gold catalysts were highly selective (>90%) and the carbon balance was close to 100%. This high selectivity was even confirmed in the hydrogenation of 1-hexyne + 1-hexene, at fixed conditions of

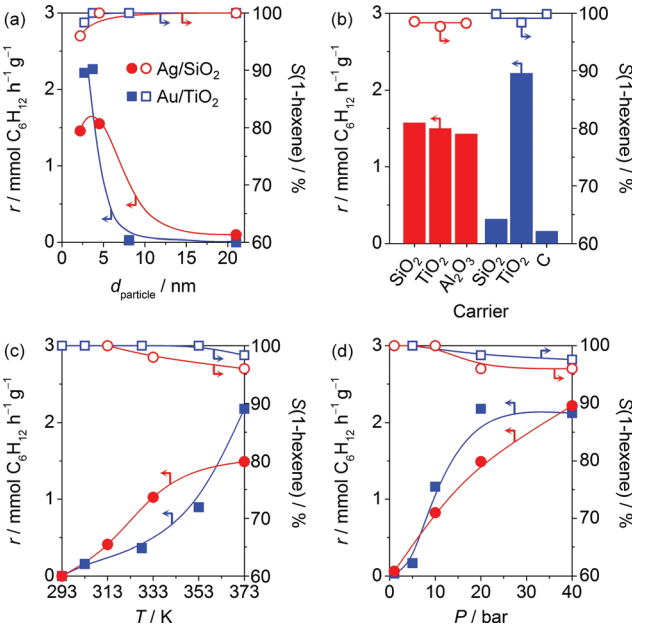

Fig. 3 Hydrogenation of 1-hexyne over the silver and gold-based catalysts as a function of the average particle size (a), support (b), temperature (c), and pressure (d). The particle size effect was studied at T = 373 K and P = 20 bar over catalysts **A**, **B**, **C**, **G**, **H**, **I** and **J** (Table 1). The effect of the carrier was investigated at T = 373 K and P = 20 bar over catalysts **A**, **D**, **E**, **F**, **G** and **K**. The influence of the temperature (pressure) was assessed at P = 20 bar (T = 373 K) over catalysts **A** and **G**. All reactions were conducted at F(liquid) = 0.3 cm^3 min^{-1} and $F(H_2)$ = 60 cm^3 min^{-1}.

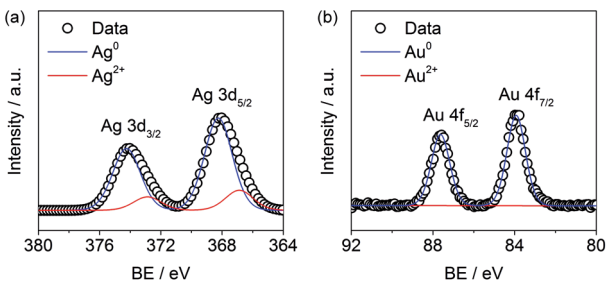

Fig. 2 Ag 3d (a) and Au 4f (b) core level XPS spectra of catalysts **A** (a) and **G** (b) in Table 1.

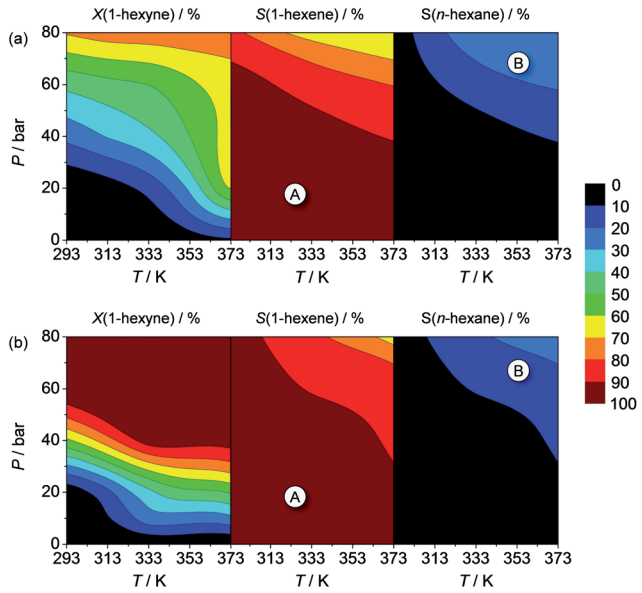

Fig. 4 Contour plots showing the influence of temperature and pressure on the hydrogenation of 1-hexyne over catalysts **A** (a) and **G** (b) in Table 1. The reactions were conducted at F(liquid) = 0.3 cm^3 min^{-1} and $F(H_2)$ = 60 cm^3 min^{-1}.

temperature and pressure (373 K, 10 bar), demonstrating that the reduction of the double bond is impeded over Ag and Au, consistently with the literature.[10a] The catalyst stability in 1-hexyne hydrogenation has been additionally verified in a long run (Fig. 5), at a degree of alkyne conversion of <40%. No drop in activity and alkene selectivity can be detected during 5 h on stream. Finally, comparing the lab-made catalyst **G** with a commercial 1 wt% Au/TiO_2, no significant difference in activity could also be observed for the hydrogenation of 1-hexyne (Fig. S3†), indicating the reproducibility of the catalytic performance.

The selectivity of the silver and gold nanoparticles have been evaluated in the hydrogenation of acetylenic compounds of varying complexity and compared to the Lindlar (Pd–Pb),[4] NanoSelect™ (Pd–HHDMA),[8a] and ceria (CeO_2/TiO_2)[15] catalysts. Table 2 compares the product selectivity for each compound and catalytic system under kinetic conditions. Since proper kinetic investigations enabling to capture intrinsic selectivity differences among the catalysts should be conducted at moderate degree of conversion, the tests in Table 2 were performed at a conversion of the acetylenic substrate of *ca.* 30%. In the hydrogenation of linear, internal alkynes (3-hexyne, entry 1), the Ag and Au catalysts yield the *cis*-alkene with high selectivity (90%), proving that *cis*/*trans* isomerisations are impeded. However, the selectivity to 3-hexene is somewhat higher over the Lindlar, NanoSelect™, and ceria catalysts (97–100%). On the other hand, in the hydrogenation of alkynes containing multiple unsaturations (valylene, entry 2, and phenylacetylene, entry 3), silver and gold catalysts provide comparable degrees of selectivity to palladium (92–100%), and these results are only slightly lower than those over ceria (100%). In particular, the absence of the 3-methyl-1-butyne product for the Ag- and Au-catalysed valylene hydrogenation suggests that C=C unsaturations do not adsorb on the active phase (thermodynamic selectivity) and/or the reduction of a double bond presents a large energy barrier (kinetic selectivity). In the case of functionalised alkynes, the hydrogenation of 2-methyl-3-butyn-2-ol (entry 4), 9-dodecyn-1-ol (entry 5), and 1,1-diphenyl-2-propyn-1-ol (entry 6) occur both stereo and chemoselectively, exhibiting degrees of selectivity close to 100%. These results exceed the performance of the NanoSelect™ catalyst, which in some cases is inactive because of the presence of the outer capping layer of HHDMA, limiting the access and adsorption of bulky substrates on the catalyst surface.[9] Finally, in the hydrogenation of acetylenic compounds containing a ketonic group, such as 3-butyn-2-one (entry 7), the supported silver and gold nanoparticles are much less selective than Lindlar and NanoSelect™. This result demonstrates that the ketone interacts with the surface of silver and gold, in line with earlier studies showing the excellent performance of Ag and Au-based nanocatalysts in the hydrogenation of α,β-unsaturated aldehydes and ketones.[18] Finally, we should comment on the different activity of Ag and Au in comparison with the Pd catalysts. In fact, the operating conditions over gold and silver in term of higher temperature and pressure (Fig. 6) and longer contact times are a clear indication of the much lower reactivity of the former metals (from the data in Table 2, it is possible to estimate that the reaction rates of poisoned Pd is 40 times higher than that of the Ag and Au counterparts). However, differently from the gas-phase alkyne hydrogenation for olefin purification, liquid-phase operation in the fine chemical industry favours operation at maximized selectivity, even if the conversion is limited.[3] Therefore, the high olefin selectivity attained over Ag and Au are highly attractive.

Finally, palladium catalysts efficiently work at ambient conditions, but require metal poisoning (*i.e.*, lead on the Lindlar catalyst) and modifiers (*i.e.*, HHDMA on the NanoSelect™ catalyst) to suppress their activity, avoiding over-hydrogenation to the alkane and oligomerisation. As shown, these modifiers not only lower the utilisation of the expensive active phase but can even block the catalyst activity due to steric constraints.[9] Ceria does not require modifiers but demanding conditions of temperatures and pressures (Fig. 6). Supported silver and gold nanoparticles are also highly selective to the olefin because of the hindered activation of molecular hydrogen, which sup-

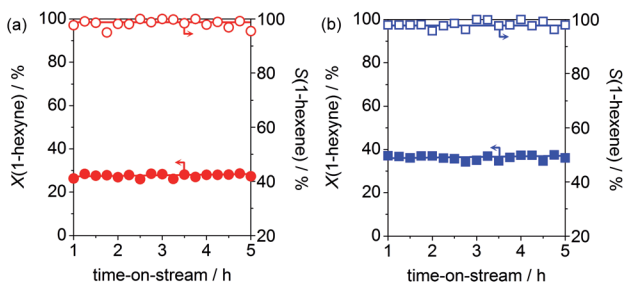

Fig. 5 Hydrogenation of 1-hexyne *versus* time-on-stream over catalysts **A** (a) and **G** (b) in Table 1. Reaction conditions: T = 373 K, P = 10 bar, F (liquid) = 0.3 cm^3 min^{-1}, and $F(H_2)$ = 60 cm^3 min^{-1}.

Table 2 Hydrogenation of acetylenic compounds over various catalysts

			Selectivity (%)[a]				
			Ag/SiO_2[b]	Au/TiO_2[c]	Pd–Pb/$CaCO_3$	Pd–HHDMA/C	CeO_2/TiO_2
Entry	Reactant	Product	T = 373 K, P = 10 bar	T = 373 K, P = 10 bar	T = 293 K, P = 1 bar	T = 293 K, P = 1 bar	T = 413 K, P = 40 bar
1		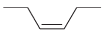	89	94	100	97	100
2			93	91	92	93	54
3	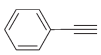		100	96	98	100	100
4			100	100	83	100	100
5	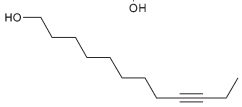	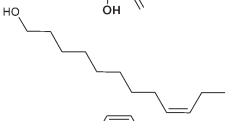	87	87	86	Inactive	100
6	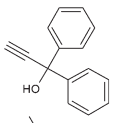	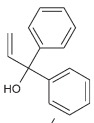	96	100	100	Inactive	100
7			67	68	97	85	—

[a] Selectivity to product at 30% alkyne conversion. [b] Catalyst **A** in Table 1. [c] Catalyst **G** in Table 1.

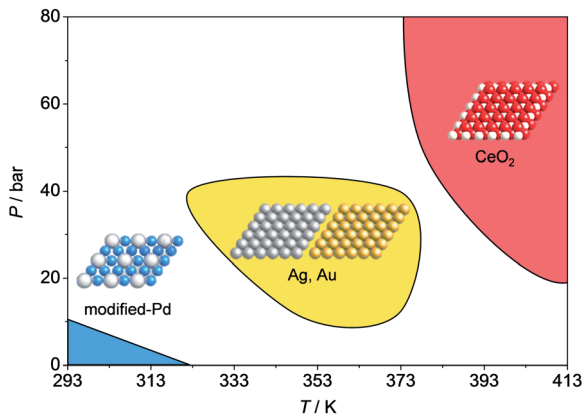

Fig. 6 Operating window (temperature and pressure) of various selective catalysts for the continuous-flow three-phase hydrogenation of acetylenic compounds.

presses the formation of hydrides.[10,11] However, the absence of poisons on the metallic surface renders them suitable for hydrogenating long-chained substrates and brings fundamental and practical simplifications in the manufacture and characterisation of these materials, compared to state-of-the-art alloyed catalysts. Besides, the mild reaction conditions of supported Ag and Au nanoparticles (313–373 K, 10 bar) in relation to the temperatures (293–313 K) and pressures (10 bar) applied in industrial practice[3] and the higher intrinsic activities obtained over the silver samples open promising perspectives for the use of these metals as sustainable alternatives to modified-Pd, also based on the fact that silver is much cheaper (19.37 USD per oz)[19] than gold and palladium (1296 and 811 USD per oz, respectively).[19]

Conclusions

Silver and gold nanocatalysts with variable average particle size (2–21 nm) were prepared, characterised, and evaluated in the three-phase semi-hydrogenation of functionalised alkynes under different temperatures (232–373 K) and pressures (1–40 bar). The alkyne conversion was maximal for catalysts featuring small nanoparticles (<5 nm), most likely because of their higher concentration of low-coordinated surface sites. In the case of silver, the activity was only slightly affected by the type of carrier; on the other hand, the gold nanoparticles were especially active when deposited on titania, probably owing to strong metal–support interactions. Both metals showed remarkable stereo and chemoselectivity in the hydrogenation of functionalised alkynes and, in some cases, the catalytic performance was competitive with that of poisoned palladium nanoparticles. However, the simplicity of preparing and characterising bare metal nanoparticles, the low-cost of silver, as well as the mild reaction conditions for the selective behaviour of these metals (313–373 K, 10 bar) are of fundamental relevance, providing insights for the design of improved materials for alkene production.

Acknowledgements

Dr E. G. Rodrigues is acknowledged for preparing and characterising the gold-based catalysts, and Dr F. Krumeich and Dr S. Mitchell for performing the electron microscopic analyses.

Notes and references

1 R. A. Sheldon, *Green Chem.*, 2007, **9**, 1273.
2 J. Yoshida, H. Kim and A. Nagaki, *ChemSusChem*, 2011, **4**, 331.
3 W. Bonrath, J. Medlock, J. Schütz, B. Wüstenberg and T. Netscher, in *Hydrogenation*, InTech, Balterswil, 2012, p. 69.
4 H. Lindlar, *Helv. Chim. Acta*, 1952, **35**, 446.
5 (*a*) J. Wegner, S. Ceylan and A. Kirschning, *Chem. Commun.*, 2011, **47**, 4583; (*b*) M. Irfan, T. N. Glasnov and C. O. Kappe, *ChemSusChem*, 2011, **4**, 300; (*c*) C. Wiles and P. Watts, *Green Chem.*, 2012, **14**, 38.
6 M. García-Mota, J. Gómez-Díaz, G. Novell-Leruth, C. Vargas-Fuentes, L. Bellarosa, B. Bridier, J. Pérez-Ramírez and N. López, *Theor. Chem. Acc.*, 2011, **128**, 663.
7 (*a*) F. Studt, F. Abild-Pedersen, T. Bligaard, R. Z. Sørensen, C. H. Christensen and J. K. Nørskov, *Science*, 2008, **320**, 1320; (*b*) M. Armbrüster, K. Kovnir, M. Friedrich, D. Teschner, G. Wowsnick, M. Hahne, P. Gille, L. Szentmiklósi, M. Feuerbacher, M. Heggen, F. Girgsdies, D. Rosenthal, R. Schlögl and Y. Grin, *Nat. Mater.*, 2012, **11**, 690.
8 (*a*) P. T. Witte, S. Boland, F. Kirby, R. van Maanen, B. F. Bleeker, D. A. M. de Winter, J. A. Post, J. W. Geus and P. H. Berben, *ChemCatChem*, 2013, **5**, 582; (*b*) W. Long, N. A. Brunelli, S. A. Didas, E. W. Ping and C. W. Jones, *ACS Catal.*, 2013, **3**, 1700.
9 G. Vilé, N. Almora-Barrios, S. Mitchell, N. López and J. Pérez-Ramírez, *Chem.–Eur. J.*, 2014, **20**, 5926.
10 (*a*) Y. Segura, N. López and J. Pérez-Ramírez, *J. Catal.*, 2007, **247**, 383; (*b*) M. Yan, T. Jin, Y. Ishikawa, T. Minato, T. Fujita, L. Y. Chen, M. Bao, N. Asao, M. W. Chen and Y. Yamamoto, *J. Am. Chem. Soc.*, 2012, **134**, 17536; (*c*) T. Mitsudomea and K. Kaneda, *Green Chem.*, 2013, **15**, 2636.
11 (*a*) A. Sárkány and Z. Révay, *Appl. Catal., A*, 2003, **243**, 347; (*b*) G. Vilé, D. Baudouin, I. N. Remediakis, C. Copéret, N. López and J. Pérez-Ramírez, *ChemCatChem*, 2013, **5**, 3750.
12 (*a*) N. Semagina, A. Renken and L. Kiwi-Minsker, *J. Phys. Chem. C*, 2007, **111**, 13933; (*b*) N. Semagina and L. Kiwi-Minsker, *Catal. Rev.: Sci. Eng.*, 2009, **51**, 147; (*c*) B. R. Cuenya, *Thin Solid Films*, 2010, **518**, 3127.
13 A. H. Øygarden, J. Pérez-Ramírez, D. Waller, K. Schöffel and D. M. Brackenbury, Patent WO2004110622, 2004.
14 N. Dimitratos, J. A. Lopez-Sanchez, D. Morgan, A. Carley, L. Prati and G. J. Hutchings, *Catal. Today*, 2007, **122**, 317.
15 G. Vilé, S. Wrabetz, L. Floryan, M. E. Schuster, F. Girgsdies, D. Teschner and J. Pérez-Ramírez, *ChemCatChem*, 2014, **6**, 1928.
16 Y. Xia, Y. Xiong, B. Lim and S. E. Skrabalak, *Angew. Chem., Int. Ed.*, 2009, **48**, 60.
17 D. Briggs and M. P. Seah, *Practical Surface Analysis by Auger and X-ray Photoelectron Spectroscopy*, Wiley, Chichester, 1st edn, 1983, p. 26.
18 P. Claus and H. Hofmeister, *J. Phys. Chem. B*, 1999, **103**, 2766.
19 http://www.mineralprices.com/, accessed on 19 May 2014.